From fractional boundary charges to quantized Hall conductance

Manisha Thakurathi, Jelena Klinovaja, and Daniel Loss
Department of Physics, University of Basel, Klingelbergstrasse 82, CH-4056 Basel, Switzerland

We study the fractional boundary charges (FBCs) occurring in nanowires in the presence of periodically modulated chemical potentials and connect them to the FBCs occurring in a two-dimensional electron gas in the presence of a perpendicular magnetic field in the integer quantum Hall effect (QHE) regime. First, we show that in nanowires the FBCs take fractional values and change linearly as a function of phase offset of the modulated chemical potential. This linear slope takes quantized values determined by the period of the modulation and depends only on the number of the filled bands. Next, we establish a mapping from the one-dimensional system to the QHE setup, where we again focus on the properties of the FBCs. By considering a cylinder topology with an external flux similar to the Laughlin construction, we find that the slope of the FBCs as function of flux is linear and assumes universal quantized values, also in the presence of arbitrary disorder. We establish that the quantized slopes give rise to the quantization of the Hall conductance. Importantly, the approach via FBCs is valid for arbitrary flux values and disorder. The slope of the FBCs plays the role of a topological invariant for clean and disordered QHE systems. Our predictions for the FBCs can be tested experimentally in nanowires and in Corbino disk geometries in the integer QHE regime.

I. INTRODUCTION

Topological phases in condensed matter physics have gained considerable interest over the past decades, which was triggered by the experimental discovery of the integer as well as of the fractional quantum Hall effect (QHE) [1–8]. Fractionalization of charges has been discussed in different topological systems and can emerge for various reasons. In the fractional QHE, strong electron-electron interactions are responsible for generating fractional excitations [9–12]. However, fractional charges can occur also in noninteracting models as was first proposed in the Jackiw-Rebbi model [13,14] and later in the Su-Schrieffer-Heeger model [15–17]. In these models, the fractional charge of $e/2$ is localized at domain walls [14,16]. Afterwards, such models were extended to describe also fractional charges localized at the boundaries [18–20]. In contrast to fractional excitations in the fractional QHE, which were investigated in transport and shot-noise experiments [21–24], the fractional boundary charges (FBCs) are far less explored experimentally, which is partially connected to the fact that the Jackiw-Rebbi and Su-Schrieffer-Heeger models are toy models. However, in recent years, there was a revival of interest in FBCs with several models being proposed that are realizable in condensed matter systems [25–39].

In this work, we first focus on the properties of FBCs in one-dimensional nanowires (NWs) with periodically modulated chemical potentials (see Fig. 1). Such a system is known to host in-gap bound states for a certain set of the offset phases α, if the period of modulation λ is tuned to half of the Fermi wavelength $\lambda = \pi/k_F$, where k_F is the Fermi wave vector [40]. However, as was shown subsequently, the FBCs in such setups do not not rely on the presence of such in-gap bound states and the FBCs are well defined even if the bound states are absent [41]. Remarkably, the FBCs in NWs turned out to be also very stable against moderate disorder [41]. All these

properties motivate us to study the FBCs in greater detail and, in particular, to generalize these findings to the regime in which the amplitude of the chemical potential modulation is comparable to the Fermi energy, thereby going beyond previous studies restricted to the perturbative regime [41]. In addition, we consider regimes in which λ is an integer multiple of half of the Fermi wavelength $\lambda = \nu\pi/k_F$, with ν being a positive integer. Interestingly, also in this case, we find that there is a gap opening at the Fermi level. Moreover, this gap can host bound states if α is properly tuned. We also find that the FBCs are linear functions of α with the slope $c_\nu = \nu e/2\pi$, being universal and quantized in units of $e/2\pi$. Again, this quantization is extremely robust against disorder, which suggests that this slope plays the role of a topological invariant for the system.

In principle, the FBCs can be observed directly by using, for example, STM techniques to measure the charge at the ends of the NWs [41]. In this way, one can also measure the linear dependence of the FBCs on the phase offset. However, we would like to connect the slope c_ν to other well-known quantized observables. For one-dimensional systems, the behavior of the FBCs is connected to properties of quantum charge pumps that transfer a quantized charge in each pumping cycle [42–49]. However, no such connection between FBCs and transport properties has been established yet in
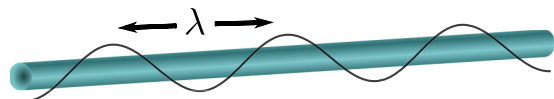

FIG. 1. Sketch of a one-dimensional NW (blue cylinder) in the presence of a chemical potential (black) which is periodically modulated, for example, by gates, with period λ.

245404-1

two-dimensional QHE setups. In this work, we attempt to fill this gap by connecting the quantized slope of the FBCs to quantized values of the Hall conductance in the integer QHE regime. To achieve this, we make use of the formal mapping between a one-dimensional (1D) NW with periodic modulations and a two-dimensional (2D) QHE system [50]. Such methods of dimensional extension or reduction were successfully employed to study properties of quasicrystals in different systems [45,48,49]. If periodic boundary conditions are imposed along one direction, giving rise to a cylinder topology, the FBC can be controlled by flux insertion, thereby implementing the Laughlin setup [4]. Physical realizations of such a cylinder topology are given by Corbino disks in the QHE regime [8,51–56]. Quite remarkably, the FBCs depend linearly on this flux and again with a slope c_ν that is universal and quantized like in the single NW case. We show that this slope quantization is again very stable against disorder in the whole sample (including the edges) as long as the bulk gaps are not closed. Finally, the quantized values of the slope c_ν can be connected to the quantized values of the Hall conductance $\nu e^2/h$. This connection clearly illustrates that all the occupied bulk states (via contributing to the FBCs) contribute to the Hall conductance and not just the edge states (which are responsible for the jump from one quantum Hall plateau to another). In addition, the approach via FBCs shows that the Hall current changes continuously with an arbitrary change in the flux, unlike in the Laughlin argument where the Hall current is determined only for integer multiples of the flux quantum $\varphi_0 = h/e$ [4]. Importantly, since our results are valid in the presence of disorder in the whole sample, we can consider the universal quantized slope of the FBCs, c_ν, as a topological invariant in integer QHE systems. The quantized slope can be accessed by charge measurements, thus opening up alternative ways to study QHE systems experimentally, beyond standard measurements via charge currents.

The outline of the paper is as follows. In Sec. II, we introduce the model consisting of a single one-dimensional NW with periodically modulated chemical potential and calculate the FBCs for different values of the phase offset as well as for different number of filled bands. We identify characteristic features of the FBCs numerically and, in addition, provide analytical arguments to explain them. In Sec. III, we map the aforementioned model to an integer QHE system consisting of an array of coupled NWs in the presence of magnetic field applied perpendicular to the NW plane. Next, we study the local particle density and the FBCs for the QHE system in the presence of an external flux both in the absence (Sec. IV) and presence (Sec. V) of disorder. In Sec. VI, we relate the quantized linear slopes of the FBCs to the quantization of the Hall conductance. Finally, in Sec. VII, we conclude with a summary and outlook.

II. FBC IN SINGLE NANOWIRE

A. Model

First, we consider a one-dimensional single-subband NW. Here and in what follows, we neglect the spin degree of freedom and work with spinless electrons. The chemical potential is assumed to be periodically modulated, for example, by

external local gates, creating the charge-density-wave (CDW) type modulation [57,58] with the amplitude $2V$ and period λ along the entire length of the NW as depicted in Fig. 1. The tight-binding Hamiltonian of such a system has the following form:

$$
\begin{aligned}
H_{1D} = &-t_x \sum_{n=1}^{N-1} (\psi_{n+1}^\dagger \psi_n + \text{H.c.}) \\
&- \sum_{n=1}^{N} \left[2V \cos\left(2\pi n \frac{a_x}{\lambda} + \alpha\right) + \mu - 2t_x \right] \psi_n^\dagger \psi_n, \quad (1)
\end{aligned}
$$

where ψ_n is an annihilation operator acting on an electron located at site n of the NW of length $l = (N-1)a_x$, with N being the number of sites. The hopping amplitude t_x and the lattice spacing a_x determine the effective electron mass. The chemical potential μ is taken from the bottom of the band. The phase offset α of the CDW, defined uniquely between $(-\pi, \pi]$, sets the value of the chemical potential at the left end of the NW (at site $n = 1$).

B. Energy spectrum

If the CDW amplitude is small, $V \ll t_x$, we can study the model analytically in the continuum regime [40,59,60]. We begin by linearizing the continuum model Hamiltonian close to the Fermi momenta $\pm k_F$, defined in terms of the chemical potential as $k_F a_x = \arccos(1 - \mu/2t_x)$, and by writing the fermion operators in terms of slowly varying right and left movers denoted by $R(x)$ and $L(x)$, respectively, as

$$
\psi(x) = R(x)e^{ik_F x} + L(x)e^{-ik_F x}. \quad (2)
$$

We neglect the fast oscillating terms and rewrite the kinetic part of the Hamiltonian as

$$
H_{kin} = i\hbar v_F \int dx \, [L^\dagger(x)\partial_x L(x) - R^\dagger(x)\partial_x R(x)]. \quad (3)
$$

Here, v_F is the Fermi velocity given by $\hbar v_F = 2t_x a_x^2 k_F$. The CDW term has following form in the linearized model:

$$
\begin{aligned}
H_{CDW} = &-V \int dx [e^{2ix(\pi/\lambda - k_F) + i\alpha} + e^{-2ix(\pi/\lambda + k_F) - i\alpha}] \\
&\times R^\dagger(x)L(x) + \text{H.c.} \quad (4)
\end{aligned}
$$

Generally, such rapidly oscillating terms average out to zero unless the resonance condition $k_F = \nu \pi/\lambda$, with ν being an integer, is satisfied. We first analyze the special case $\nu = 1$ and then consider general ν. In this case, H_{CDW} couples right and left movers at the Fermi level, and as a result a gap of size $\Delta_g^{(1)} = V$ opens in the spectrum [40] (see Fig. 2).

In the basis $\tilde\psi = (R, L)$, the total linearized Hamiltonian in the resonance case ($k_F = \pi/\lambda$) has the form $H_{1D} = \int dx \, \psi^\dagger \mathcal{H} \psi$ with Hamiltonian density $\mathcal{H} = \hbar v_F \hat{k} \sigma_z - V\cos(\alpha)\sigma_x + V\sin(\alpha)\sigma_y$, where $\hat{k} = -i\partial_x$ is the momentum operator with eigenvalue k. The bulk spectrum is given by $E_\pm = \pm[(\hbar v_F k)^2 + V^2]^{1/2}$. For an infinitely long NW, no states reside inside the bulk gap as the spectrum is fully gapped for all values of k. To explore the possibility of bound states in the gap [61], we consider a finite
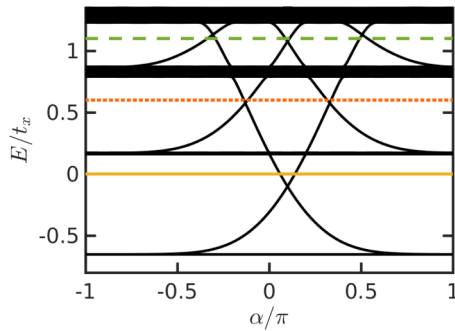
FIG. 2. Energy spectrum of a NW with CDW modulation of strength V and period λ as a function of phase offset α. Bulk gaps are opened by resonant scattering between the two Fermi points caused by the periodic modulation. If the chemical potential μ is tuned inside these gaps and the phase offset α is properly adjusted, bound states localized at the NW ends with energies inside the bulk gap emerge. The three colored horizontal lines correspond to the position of μ inside the first ($\mu/t_x = -0.1$, yellow solid line), second ($\mu/t_x = 0.5$, orange dotted line), and third ($\mu/t_x = 1$, green dashed line) bulk gap. The FBCs will be calculated at these values of μ. The parameters are chosen as $N = 600$, $V/t_x = 0.6$, $\lambda/a_x = 10$, and $\mu/t_x = -0.1$.
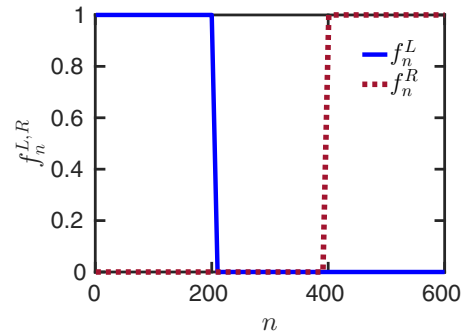

FIG. 3. The profile function f_n^L (f_n^R) is defined to capture features of the FBC at the left (right) NW end as a function of lattice site n. The used parameters are $N = 600$, $n_1 = 200$, and $n_2 = 10$.

NW of length l with the condition that $l \gg \xi$ [62], where ξ is the localization length of the bound state. Next, we impose vanishing boundary condition at the left (right) end of the NW, $x = 0$ ($x = l$), such that $R(0) + L(0) = 0$ $[R(l) + L(l)e^{-2ik_F l} = 0]$. The spectrum of the bound state localized at the left (right) edge of the NW depends on the phase offset α and is given by $\epsilon(\alpha) = V \cos(\alpha)$ $[\epsilon(\alpha) = V \cos(\alpha + 2k_F l)]$ under the constraint $\sin(\alpha) < 0$ $[\sin(\alpha + 2k_F l) > 0]$. If the latter constraints are not satisfied, there is no bound state. The corresponding wave functions have the form $\tilde{\phi} \sim \sin(k_F x) \exp(-x/\xi)$ $(\tilde{\phi} \sim \sin[k_F (x - l)] \exp[(x - l)/\xi])$ with the localization lengths defined as $\xi = -\hbar v_F/[V \sin(\alpha)]$ $(\xi = \hbar v_F/[V \sin(\alpha + 2k_F l)])$.

Next, we can generalize these results to arbitrary positive integer ν where the condition $k_F = \nu \pi/\lambda$ also allows for resonant scattering between left and right movers in higher orders of perturbation theory [63,64]. In this case, the gap is opened in the νth order of perturbation expansion and is of order of $\Delta_g^{(\nu)} \approx V^\nu/E_0^{\nu-1}$, where E_0 is the characteristic energy which depends on the chemical potential of the system. We refer to Appendix A for further details. The gap $\Delta_g^{(\nu)}$ is reduced by a factor $(V/E_0)^{\nu-1}$ in comparison with the direct gap $\Delta_g^{(1)}$, which implies that as the value of ν increases the gap decreases. The spectrum of the bound states can also be calculated in a similar way as done before for $k_F = \pi/\lambda$. However, we note here that one can directly recalculate the energy spectrum by rescaling $\alpha \to \nu\alpha$ and also $V \to \Delta_g^{(\nu)}$ (see Appendix A for more details). As an important consequence, in this perturbative regime, the spectrum of bound states at one given NW end satisfies $\epsilon(\alpha) = \epsilon(\alpha + 2\pi p/\nu)$ for $p = 0, \ldots, \nu - 1$. This feature ensures that as one changes α from $-\pi$ to π, there will be ν bound states, localized at each NW end, at any given energy inside the νth bulk gap (see Fig. 2).

As the amplitude of the CDW grows, $V \simeq t_x$, the CDW cannot be treated perturbatively anymore. The size of the bulk gaps gets larger compared to the perturbative regime up to the point at which the energy bands get flat (see Fig. 2). However, as the bulk gap never closes upon increasing V, one can conclude that the bound states are still present in the spectrum and, moreover, their number inside a given gap is also not changing. When the chemical potential lies inside the lowest gap, the bound states obtained above were discussed before in different contexts in Refs. [40,65,66]. Here, we have shown in addition that the number of bound states increases as one tunes the chemical potential inside the bulk gaps opened at higher energies. Furthermore, we also note that the commensurability relation between λ and a_x does not play any role in our setup, which is also confirmed by the analytical solutions obtained in continuum limit.

C. Fractional boundary charge

Next, we turn to the FBC in a single NW with CDW modulation. To begin with, we define the FBC at each of two NW ends as [41]

$$Q_{\nu,1d}^s = \sum_{n=1}^N f_n^s (e \langle \psi_n^\dagger \psi_n \rangle - \bar{\rho}_\nu), \qquad (5)$$

where we have subtracted from the expectation value of the charge density in the ground state at site n, $e \langle \psi_n^\dagger \psi_n \rangle$, the average bulk charge per site $\bar{\rho}_\nu$. Here, e is the electron charge. If the chemical potential is tuned inside the νth bulk gap, we have $\bar{\rho}_\nu = e \nu a_x/\lambda$. To capture the FBCs at the left ($s = L$) and right ($s = R$) NW ends separately, we introduced a profile function f^s, which has spatial support only at one of the two NW ends (see Fig. 3). Without loss of generality, we work with the following profile function defined by two cutoffs $n_1, n_2 > 0$ (for sharp transition, $n_2 = 1$):

$$f_n^L = \Theta(n_1 + n_2 - n)$$
$$- \frac{n - n_1}{n_2}[\Theta(n - n_1) - \Theta(n - n_1 - n_2)], \qquad (6)$$

where $\Theta(x)$ is the Heaviside step function. The profile function at the right f_n^R is mirror symmetric to the function at
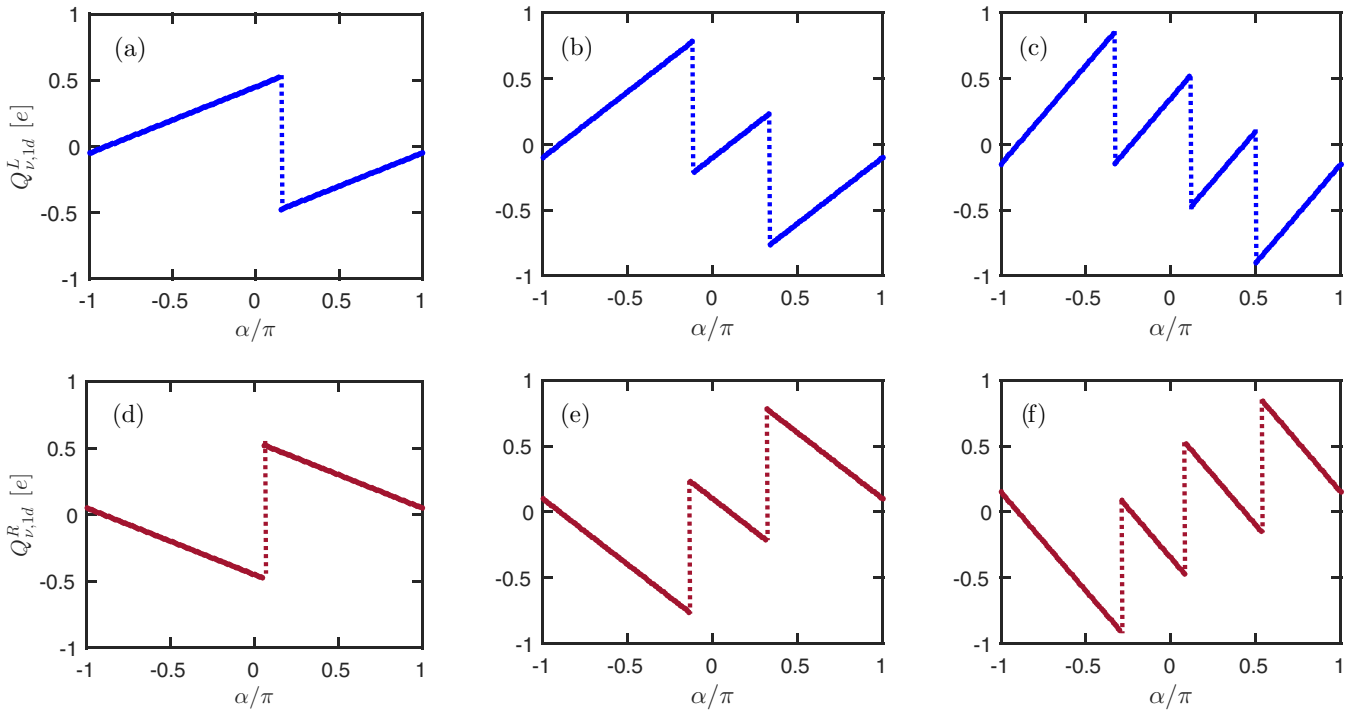
FIG. 4. The FBCs, $Q^L_{\nu,1d}$ [blue, (a)–(c)] and $Q^R_{\nu,1d}$ [red, (d)–(f)], measured in the units of electron charge e as a function of the phase offset α obtained numerically for the CDW-modulated NW. The number of filled bands is controlled by the chemical potential that is tuned inside the first [(a), (d)], second [(b), (e)], or third [(c), (f)] bulk gap (see Fig. 2). The FBCs vary linearly as a function of α and the absolute value of the slope is quantized for (a),(d), (b),(e), and (c),(f) as $1/2\pi$, $2/2\pi$, and $3/2\pi$. The sign of the slope is opposite at two ends. The FBCs jump by $\pm e$ at the bound states cross the chemical potential. The parameters are chosen to be the same as in Figs. 2 and 3.

the left given by $f^L_n = f^R_{N+1-n}$, where $1 \leqslant n \leqslant N$. A well-defined FBC should be independent of the form of the profile function and of the precise choice of the two cutoffs as long as $n_1 a_x \gg \xi$ and $n_2 a_x \gg \lambda$ (see Appendix B). Note that *all* states filled up to the Fermi level contribute to the FBC including a possible bound state.

After defining the FBCs, we calculate it numerically for the left and right NW ends and for different positions of the chemical potential μ inside the νth gaps (see Fig. 4). We observe the following four salient features: (1) The FBCs change linearly as a function of the phase offset α, which allows us to define the slope of the linear function describing this dependence. (2) The slope is given strictly by the universal value $\pm e\nu/2\pi$. Thus, the slope is quantized and depends only on the number of filled bands or, in other words, on the band gap inside which the chemical potential is tuned. The position of the chemical potential inside the band gap does not affect the slope. The signs of the slope defined for the right and left FBCs are opposite. (3) The FBCs change continuously and can take positive and negative values. These values are usually bounded between $-e$ and e. (4) The FBCs jump by the amount $\pm e$ as the energy of the bound states localized at the corresponding NW end flips its sign, as one changes α. Indeed, if the bound state energy is negative (positive), the corresponding state is filled (empty), and, thus, it contributes (does not contribute) with charge e to the FBCs. Consequentially, as the bound state crosses the chemical potential, the FBCs should change by $\pm e$. The position of such jumps depends on the precise position of the chemical potential inside the νth gap. In contrast to that, the

number of jumps is determined by the number of bound states and is quantized and given by ν.

D. Linear dependence of FBCs on phase offset

In this section we discuss the functional dependence of FBCs on the phase offset α and provide analytical arguments to support the linear dependence between these two quantities established numerically in the previous subsection. For this we need to generalize the approach given in Ref. [41] for $\nu = 1$ to arbitrary integer values of ν. For simplicity, we carry out the proof in the tight-binding model description, where we also assume that λ and a_x are commensurable. However, this is not a crucial requirement and this constraint can be loosened if one switches to the continuum description. We define the total charge Q_{1d} of the NW decomposed into three parts [41],

$$Q_{1d} = Q^b_{\nu,1d} + Q^L_{\nu,1d} + Q^R_{\nu,1d}, \qquad (7)$$

where $Q^b_{\nu,1d} = N \bar{\rho}_\nu = N e \nu a_x / \lambda$ is the charge of the constant (uniform) bulk background and $Q^{L/R}_{\nu,1d}$ the FBCs at the left/right end of the NW. In what follows, the chemical potential μ is assumed to be inside the νth bulk gap, such that Q_{1d} is an integer multiple of e. Below, we study the change in the FBCs, $Q^{L,R}_{\nu,1d}$, upon changing the system size N and the phase offset α. First, we note that in long NWs $Q^R_{\nu,1d}$ does not change if one extends the NW by one full period of the CDW, i.e., by changing the size from N to $N + \lambda$. Thus, $Q^R_{\nu,1d}$ must be a function of $\delta = N \bmod(\lambda/a)$. Let us now consider the following steps.

(1) We extend the NW at the right end by one site such that the number of sites increases to $N + 1$. Therefore, the bulk charge $Q_{\nu,1d}^b$ increases by $\nu e a_x/\lambda$. As Q_{1d} can take only integer values, this change should be compensated by the FBCs and, thus, $Q_{\nu,1d}^{L,R}$ have to decrease by $\nu e a_x/\lambda$. However, the FBC at the left NW end $Q_{\nu,1d}^L$ should remain unaffected by manipulations on the right NW end, thus,

$$Q_{\nu,1d}^R(N + 1) - Q_{\nu,1d}^R(N) = -\nu e a_x/\lambda. \tag{8}$$

Here, the change in the FBC is defined up to $\pm e$.

(2) We note that, if one readjusts α, one can compensate for the shift of the right end by one site and keep $Q_{\nu,1d}^R$ unchanged. This would require to change α as $\alpha \rightarrow \alpha - 2\pi a_x/\lambda$. Thus, $Q_{\nu,1d}^R$ is not a function of two independent parameters α and δ but only of their combination, i.e.,

$$Q_{\nu,1d}^R(\delta, \alpha) = Q_{\nu,1d}^R\left(\frac{a_x \delta}{\lambda} + \frac{\alpha}{2\pi}\right). \tag{9}$$

From Eq. (8) we conclude that $Q_{\nu,1d}^R$ is a linear function of δ. Hence, it follows from Eq. (9) that the FBC, $Q_{\nu,1d}^R$, is also a linear function of α,

$$Q_{\nu,1d}^R(\alpha) = -c_\nu \alpha + C^R, \tag{10}$$

where the slope is determined by $c_\nu = e \nu/2\pi$, in full agreement with our numerical findings (see Fig. 4). The piecewise constant function C^R will be neglected in what follows. We just note that C^R jumps by e as one of the bound states crosses the chemical potential upon changing α. The number of the bound states at each end is given by ν. Thus, the total change of C^R as α is changed continuously by 2π is $e\nu$. This ensures the periodicity of the FBC, $Q_{\nu,1d}^R(\alpha) = Q_{\nu,1d}^R(\alpha + 2\pi)$.

As one changes α, the bulk contribution $Q_{\nu,1d}^b$ to the total charge stays constant. Thus, the sum of the two FBCs, $Q_{\nu,1d}^R + Q_{\nu,1d}^L$, must also remain unchanged unless there is a bound state crossing the chemical potential. This means that the left FBC, $Q_{\nu,1d}^L$, is also a linear function of α with the same absolute value of the slope c_ν. However, the sign of the slope is opposite such that $Q_{\nu,1d}^L$ ($Q_{\nu,1d}^R$) increases (decreases) as α is increased. This is again in full agreement with the numerical results (see Fig. 4).

We note that our model can be considered as a generalization of Jackiw-Rebbi model. However, first, in our case the values of the FBC are not restricted to $e/2$, which is the outcome of particle-hole symmetry in the Jackiw-Rebbi model, and can take continuous set of values, which was already noticed previously in Ref. [41]. Second, this set of values has a large range, meaning that the difference between the maximum FBC and the minimum FBC is between e and νe, whereas it is always strictly e in the Jackiw-Rebbi model.

III. MAPPING FROM NW TO QHE SYSTEM

We extend now our considerations to 2D systems in the QHE regime. First, we consider the clean case and subsequently add disorder. The setup considered in Sec. II, which consists of a single NW with periodically modulated chemical potential, can be mapped to a system of tunnel-coupled NWs in a uniform magnetic field as follows [45,50,67–69]. We consider a finite array of M tunnel-coupled NWs, in the presence of a magnetic field which is applied perpendicular to the plane
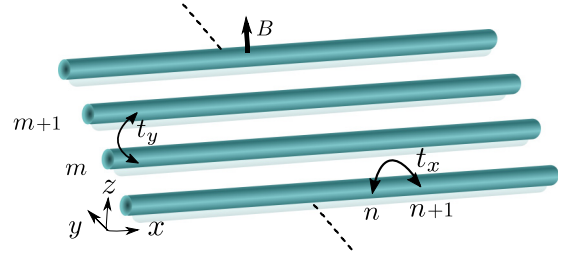

FIG. 5. An array of one-dimensional tunnel-coupled NWs (blue cylinders) is placed in the xy plane. The external magnetic field **B** is applied along the z direction. The electron tunnels with an amplitude t_x (t_y) within the NW (between two neighboring NWs). The array models an integer QHE for appropriate values of the B field.

of the NWs, i.e., along the z direction, as shown in Fig. 5. We work in the Landau gauge and choose the corresponding vector potential to be along the y direction, in Cartesian coordinates $\mathbf{A} = B x \hat{y}$. Therefore, the Peierls phase, which the electron accumulates as it tunnels between NWs, is given by $\phi(x) = (e/\hbar) \int \mathbf{A} \cdot d\mathbf{l} = (eB a_y/\hbar) x = (2\pi/\lambda) x$, where we have introduced $\lambda = h/eB a_y$ and used $d\mathbf{l} = dx \hat{x} + dy \hat{y} + dz \hat{z}$. In the discretized model of the NW consisting of N sites, we have $x = n a_x$, with $1 \leqslant n \leqslant N$ being an integer. Here, a_x and a_y are the lattice spacings along x and y directions, respectively. The corresponding tight-binding Hamiltonian for this NW array is given by

$$H = \left[-t_x \sum_{(n,m)=(1,1)}^{(N-1,M)} \psi_{n+1,m}^\dagger \psi_{n,m} \right. $$
$$\left. - t_y \sum_{(n,m)=(1,1)}^{(N,M-1)} e^{i 2\pi n a_x/\lambda} \psi_{n,m+1}^\dagger \psi_{n,m} \right] + \text{H.c.}$$
$$- (\mu - 2t_x) \sum_{(n,m)=(1,1)}^{(N,M)} \psi_{n,m}^\dagger \psi_{n,m}, \tag{11}$$

where μ is the chemical potential and t_x and t_y are the hopping amplitudes inside each of the NW and in-between two neighboring NWs, respectively. The annihilation operator $\psi_{n,m}$ acts on an electron located at site n of the mth NW.

Next, we impose periodic boundary conditions along the y direction and introduce tunneling t_y also between the first and Mth NWs (see Fig. 6). Thus, the momentum k_y defined along the y direction is a good quantum number and takes quantized values ranging from $-\pi/a_y$ to π/a_y in steps of $2\pi/(M a_y)$. Applying the Fourier transformation $\psi_{n,m} = (1/\sqrt{M}) \sum_{k_y} e^{-i m k_y a_y} \psi_{n,k_y}$, one can represent the Hamiltonian H [see Eq. (11)] in momentum space as $H = \sum_{k_y} H_{k_y}$, where

$$H_{k_y} = -t_x \sum_{n=1}^{N-1} (\psi_{n+1,k_y}^\dagger \psi_{n,k_y} + \text{H.c.})$$
$$- \sum_{n=1}^{N} \left[2 t_y \cos(k_y a_y + 2\pi n a_x/\lambda) + \mu - 2t_x \right] \psi_{n,k_y}^\dagger \psi_{n,k_y}. \tag{12}$$
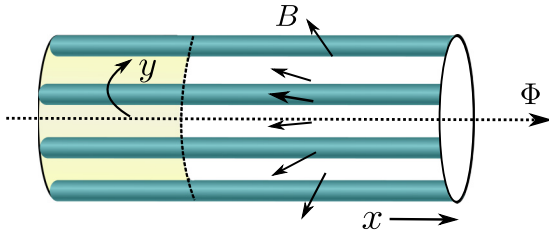
FIG. 6. Sketch of a periodic array of tunnel-coupled NWs (blue) with the topology of a cylinder oriented along the x direction. The magnetic field B points normal to the cylinder surface and is responsible for bringing the setup into the QHE regime. An external flux Φ is applied along the cylinder axis and, being changed in time, induces an electromotive force $\mathcal{E}_y$ in azimuthal direction y. For the calculation of the FBC and the Hall conductance, we focus on the patch (yellow) of area $\mathcal{A}$ localized at the left boundary of the system.

This Hamiltonian H_{k_y} exactly matches the Hamiltonian for the one-dimensional CDW modulated NW [see Eq. (1)] upon the substitutions $k_y a_y \rightarrow \alpha$ and $t_y \rightarrow V$. We note that now the entire 2D system decomposes into a set of M-independent 1D systems. The phase offset α plays the role of the momentum k_y. The amplitude of the CDW, V, is replaced by the tunneling amplitude t_y. The period of the CDW modulation of the chemical potential, being set by the strength of the applied magnetic field, is given by $\lambda = h/eB\, a_y$. With these substitutions we can interpret the spectrum shown in Fig. 2 as the dispersion (E as function of k_y) of a two-dimensional electron gas in the QHE regime with pertinent gaps [45,50]. For the isotropic case $t_x = t_y$, we recover the standard Landau levels for the integer QHE. Finally, the ν bound states of the CDW modulated NW case are mapped to ν dispersive chiral QHE edge states (see also Fig. 2).

IV. FBC IN QHE SYSTEM WITH FLUX

In the foregoing section, we established the connection between the 1D CDW-modulated NW and an array of tunnel-coupled NWs in the QHE regime. Now, we are in the position to introduce the FBC for the 2D system. In the 1D case, the FBC depends on the phase offset α, which maps to the momentum k_y in the 2D setup. While α can be controlled experimentally and tuned to different but fixed values, in any finite 2D system all bulk states with different momentum k_y compose the ground state, and, thus, they all contribute to the FBCs. Hence, we should revisit the concept of FBCs in 2D.

First, we introduce the particle density $\gamma_{n,m}$ at the site n of the mth NW defined as

$$\gamma_{n,m} = \langle \psi_{n,m}^\dagger \psi_{n,m} \rangle. \qquad (13)$$

Here, the expectation value is calculated in the ground state of the system. In the 1D case, even far away from the NW ends, the charge density is nonuniform over the CDW period λ. In the 2D case, however, the charge density is uniform in the bulk due to the global translational invariance (see Fig. 7). Thus, in 1D we were forced to compensate for this nonuniformity in the definition of the FBCs by introducing the second cutoff n_2 in the profile function $f_n^{R,L}$ [see Eq. (6)]. In contrast to that, in the 2D setup we can work with $n_2 = 1$

in the profile function $f_n^{R,L}$ and just make sure that $n_1 a_x$ exceeds the localization length of the QHE edge states. These considerations allow us to introduce the FBCs, $Q_{\nu,2d}^s$, for the 2D setup as follows:

$$Q_{\nu,2d}^s = \sum_{(n,m)=(1,1)}^{(N,M)} f_n^s \left(e \langle \psi_{n,m}^\dagger \psi_{n,m} \rangle - \rho_\nu \right). \qquad (14)$$

Here, $s = R, L$ labels the FBC at the right and left boundaries of the system, respectively. The index ν indicates the position of the chemical potential inside the νth bulk gap with the bulk charge per site given by ρ_ν. For simplicity, we work with the same profile function f_n^s for all NWs [see Eq. (6)]. We have checked that this choice does not affect our results.

Next, we impose periodic boundary conditions along the y direction, giving rise to a cylinder topology (see Fig. 6). In addition, we add an external flux Φ. The flux is created by an additional external magnetic field B' aligned along the x axis. The corresponding vector potential $\mathbf{A}'$ is chosen to be along the y axis, $\mathbf{A}' = (B'R/2)\,\hat{y}$, where $R = Ma_y/2\pi$ is the radius of the cylinder. The total flux penetrating the cylinder is defined as $\Phi = \int \mathbf{A}' \cdot d\mathbf{l} = \pi R^2 B'$.

The corresponding Hamiltonian in the tight-binding model is defined as

$$H^\theta = \left[-t_x \sum_{(n,m)=(1,1)}^{(N-1,M)} \psi_{n+1,m}^\dagger \psi_{n,m} \right.$$
$$\left. - t_y\, e^{i\,\theta/M} \sum_{(n,m)=(1,1)}^{(N,M)} e^{i\,2\pi n a_x/\lambda} \psi_{n,m+1}^\dagger \psi_{n,m} \right] + \text{H.c.}$$
$$- (\mu - 2t_x) \sum_{(n,m)=(1,1)}^{(N,M)} \psi_{n,m}^\dagger \psi_{n,m}, \qquad (15)$$

where $\theta/M = (e/\hbar) \int \mathbf{A}' \cdot d\mathbf{l} = e\,B' R\, a_y/(2\hbar) = 2\pi\,\Phi/(\varphi_0 M)$ is the Peierls phase that the electrons acquire by tunneling between two neighboring NWs. Here, $\varphi_0 = h/e$ is the flux quantum. For simplicity of notations, we identify the $(M+1)$th NW with the first NW.

By applying the Fourier transformation and introducing the momentum k_y, we again find that the 2D Hamiltonian can be represented as a sum of independent 1D Hamiltonians in momentum space $H^\theta = \sum_{k_y} H_{k_y}^\theta$, where

$$H_{k_y}^\theta = H_{k_y}(k_y a_y \rightarrow k_y a_y + \theta/M). \qquad (16)$$

By changing the flux Φ through the cylinder, one can effectively shift the momentum k_y.

If the system is periodic along the y direction (as assumed), the particle density $\gamma_{n,m}^\theta$ is independent of the NW index m, $\gamma_{n,m}^\theta \equiv \gamma_n^\theta$ (see Fig. 7). Here, we have introduced the dependence of the particle density on the flux phase θ. Of course, this dependence is only significant at the boundaries of the system, as the bulk value of the particle density ρ_ν/e is a constant determined by the position of the chemical potential inside the νth bulk gap, as shown for $\nu = 1$ [see Figs. 7(a)–7(c)]. We obtain similar results for $\nu = 2$ and 3 (see Appendix C).

Numerically, one can easily show that the FBCs, $Q_{\nu,2d}^s(\theta)$, depend linearly on the flux phase θ (see Fig. 7). The slopes at
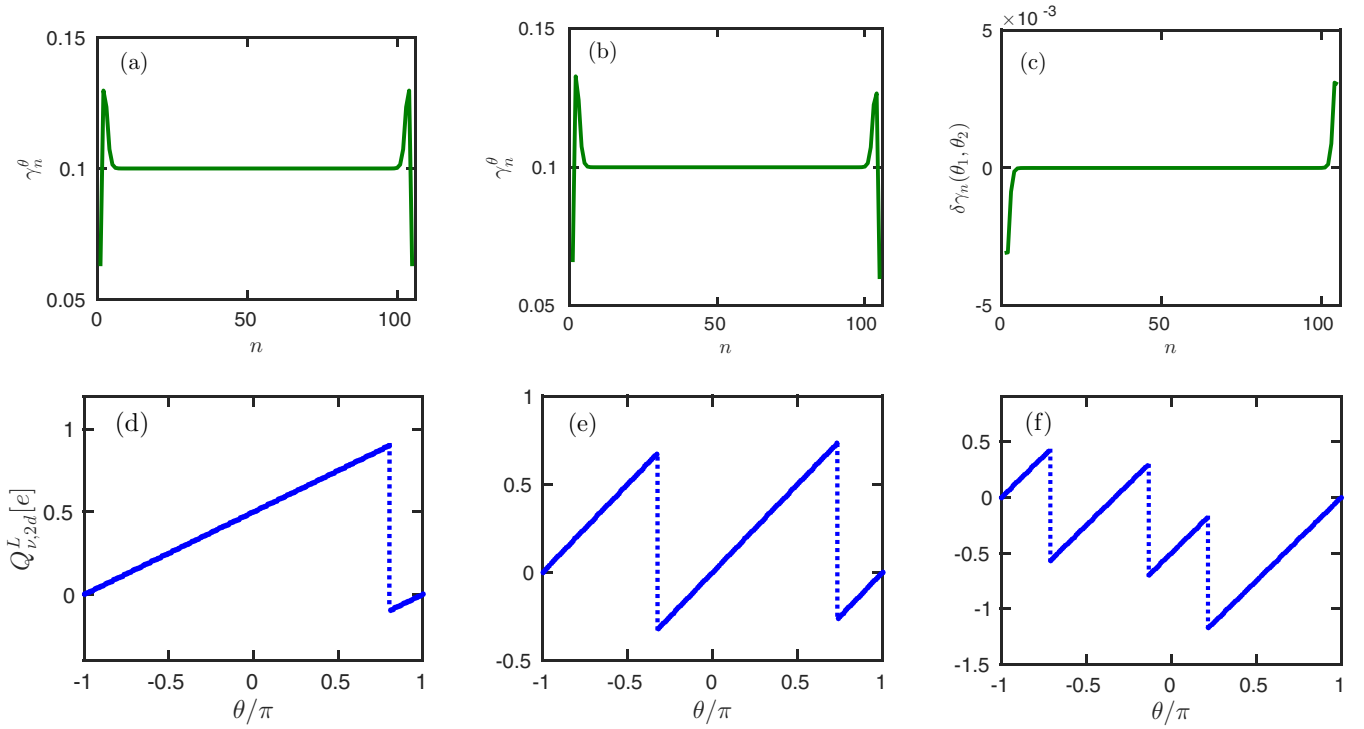
FIG. 7. Local particle density γ_n^θ for the QHE setup with chemical potential being tuned inside the first bulk gap ($\mu/t_x = -0.1$) as a function of the position along the NW for two values of the flux phase: (a) $\theta_1 = 0$ and (b) $\theta_2 = 0.9$. In (c), we plot the difference in the local particle densities $\delta\gamma_n(\theta_1, \theta_2) = \gamma_n^{\theta_1} - \gamma_n^{\theta_2}$ calculated at these two values of θ. The bulk value of γ_n^θ is universal and depends only on the number of filled bands. As a result, γ_n^θ is sensitive to the flux only at the boundaries, which results in the dependence of the FBCs on θ. The FBCs, $Q_{v,2d}^{R,L}$, change linearly as a function of the flux. The linear slope $c_v = ve/2\pi$ is perfectly quantized and the FBCs show all the four salient features described in Sec. II, now as a function of flux phase θ. The chemical potential μ is tuned inside the (d) first ($\mu/t_x = -0.1$, $v = 1$), (e) second ($\mu/t_x = 0.5$, $v = 2$), (f) third ($\mu/t_x = 1$, $v = 3$) bulk gap. The parameters are fixed as $t_y/t_x = 0.6$, $\lambda/a_x = 10$, $N = 105$, $M = 20$, $n_1 = 20$, and $n_2 = 1$.

the right and left boundaries are opposite,

$$Q_{v,2d}^R = -c_v\theta + C^R; \quad Q_{v,2d}^L = c_v\theta + C^L, \qquad (17)$$

and depend solely on the fact that the chemical potential is positioned inside the vth bulk gap $c_v = e\,v/2\pi$. To ensure the 2π periodicity of the FBC, again there must be v jumps of size $\pm e$ as the flux phase θ changes by 2π. This feature is again ensured by the nonuniversal piecewise constant functions $C^{R,L}$. In addition, we have checked that the ratio between two hopping amplitudes t_y/t_x does not play any role. All salient features of FBCs are robust against variations in the hopping amplitude t_y/t_x between the NWs (see Appendix D). In what follows, we work with $t_y/t_x = 0.6$ that is somewhere in-between the fully isotropic and strongly anisotropic limits.

The linear dependence of the FBCs on θ can also be understood analytically by using the mapping to the CDW-modulated NW. By applying the Fourier transformation to the definition of the FBCs, $Q_v^s(\theta)$, we arrive at $Q_{v,2d}^s(\theta) = \sum_{k_y} Q_{k_y}^s(\theta)$, where $Q_{k_y}^s$ is the FBC defined for an effectively 1D Hamiltonian $H_{k_y}^\theta$. Making use of Eq. (10) for the FBCs in 1D systems, in which we replace α by $k_y a_y + \theta/M$, we arrive at Eq. (17). We note that, as the sum runs over all M values of quantized momentum k_y, i.e., over the entire Brillouin zone, such that $\sum_{k_y} k_y a_y = 0$, while $\sum_{k_y} \theta/M = \theta$. This confirms

the linear dependence of the FBCs on the flux phase θ with the universal slope $c_v = e\,v/2\pi$.

V. FBC AND DISORDER IN QHE REGIME

In previous sections, for our analytical arguments, the periodicity of the system was crucial in order to establish the linear dependence of the FBCs, $Q_{v,2d}^s$, on the flux phase θ. However, in realistic samples, disorder can be substantial and break this periodicity so that k_y is no longer a good quantum number. Thus, it is crucial to check the stability and universality of the linear slopes in the FBCs as a function of flux also in the presence of disorder, where the disorder is allowed to be very general, in particular, to be present in the entire 2D system including the edges. This can be easily done numerically in the tight-binding model, where we add an onsite disorder term $\mu_{n,m}^{\text{dis}}$ characterized by a normal distribution, where the mean value, without loss of generality, is fixed to zero, while the standard deviation σ_d controls the distribution of the values of $\mu_{n,m}^{\text{dis}}$:

$$H_{\text{dis}} = \sum_{(n,m)=(1,1)}^{(N,M)} \mu_{n,m}^{\text{dis}}\, \psi_{n,m}^\dagger \psi_{n,m}. \qquad (18)$$

The full tight-binding Hamiltonian takes the form $H_{\text{tot}} = H^\theta + H_{\text{dis}}$, where H^θ is given by Eq. (15). We again first
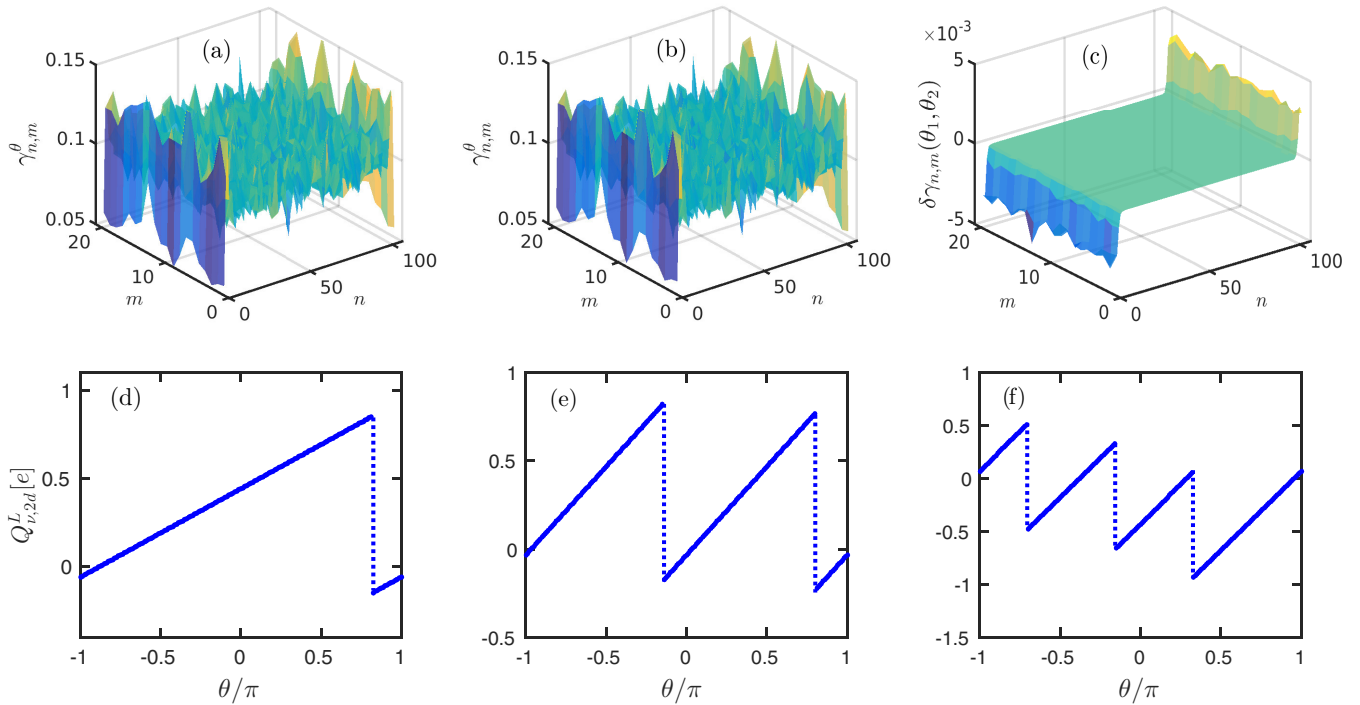
FIG. 8. The same as in Fig. 7, however, in the presence of strong disorder modeled by onsite fluctuations of the chemical potential with standard deviation $\sigma_d/t_x = 0.1$. The spatial distribution of the particle density $\gamma^\theta_{n,m}$ [(a) $\theta_1 = 0$ and (b) $\theta_2 = 0.9$] is nonuniform even in the bulk due to disorder. However, as in the clean case, the particle density depends on θ only at the boundaries of the system. Indeed, as seen from (c), the difference $\delta\gamma_{n,m}(\theta_1, \theta_2) = \gamma^{\theta_1}_{n,m} - \gamma^{\theta_2}_{n,m}$ is zero in the bulk but finite at the boundaries. (d)–(f) The left FBC ($Q^L_{\nu,2d}$) shows exactly the same dependence on the magnetic phase θ as in the clean case [compare with Figs. 7(d)–7(f)]. This demonstrates the robustness of the linear slope of FBCs to disorder.

calculate numerically the particle densities $\gamma^\theta_{n,m}$ for different values of magnetic flux (see Fig. 8). In contrast to the clean case, $\gamma^\theta_{n,m}$ are not constant anymore even in the bulk of the system, i.e., away from the sample boundaries. However, the mean value of $\gamma^\theta_{n,m}$ stays close to the clean bulk limit value ρ_ν/e. Again, the largest deviations from ρ_ν/e are observed at the boundaries of the system. Surprisingly, if one focuses on the changes in the particle densities $\gamma^\theta_{n,m}$ as the flux phase θ is adjusted for the same configuration of disorder, one notices that $\gamma^\theta_{n,m}$ in the bulk of the system is independent of the magnetic flux value. By calculating the difference of particle densities for two different values of flux phases θ_1 and θ_2, $\delta\gamma_{n,m}(\theta_1, \theta_2) = \gamma^{\theta_1}_{n,m} - \gamma^{\theta_2}_{n,m}$, we find that $\delta\gamma_{n,m}(\theta_1, \theta_2)$ takes nonzero values only at the boundaries [see Fig. 8(c)]. In comparison with the clean case, the particle density $\gamma^\theta_{n,m}$ is nonuniform along the boundary as the translation invariance is broken by disorder. However, this local redistribution of the particle density along the boundary does not effect the FBCs. Importantly, also in the presence of strong disorder, $Q^{L,R}_{\nu,2d}$ reproduces a linear dependence on the flux phase θ [see Figs. 8(d)–8(f)] and Eq. (21) is valid. We note that, in what follows, we are interested in the part of the FBC, $Q^{R,L}_{\nu,2d}$, that depends on the flux phase θ. Thus, even if in the presence of strong disorder the average particle density in the bulk can deviate from the clean case value ρ_ν used in the definition of the FBC [see Eq. (14)], it does not play any role in further discussions, in which we will be interested only in differences in the FBCs, $\delta Q^{R,L}_{\nu,2d}(\theta_1, \theta_2) = Q^{R,L}_{\nu,2d}(\theta_1) - Q^{R,L}_{\nu,2d}(\theta_2)$.

Obviously, the constant ρ_ν used in Eq. (14) does not play any role as it cancels exactly in the expression for $\delta Q^{R,L}_{\nu,2d}(\theta_1, \theta_2)$. However, this allows us to explain a slight offset between the values of the FBCs obtained in the clean (see Fig. 7) and disordered (see Fig. 8) cases.

In addition, similarly to the bound states in the 1D case described above, we note that it is the chiral edge states in the QHE regime that are responsible for the finite jump in the FBCs, $Q^{R,L}_{\nu,2d}$. This jump is always in integer steps of the elementary charge e and can be understood as follows. The summation in the definition of $Q^{R,L}_{\nu,2d}$ [see Eq. (14)] runs over a length that is larger than the typical localization length (in x direction) of the edge states. Therefore, each filled edge state below the chemical potential contributes fully to the boundary charge, i.e., $e \sum_{(n,m)=(1,1)}^{(N,M)} f^s_n \langle \psi^\dagger_{n,m} \psi_{n,m} \rangle_{\text{filled}} = e$. Thus, if a filled edge state crosses the chemical potential as a function of θ, there is an integer jump in units of e in $Q^{R,L}_{\nu,2d}$. Away from such crossing points, $Q^{R,L}_{\nu,2d}$ is a smooth linear function of θ (see Fig. 8). Conversely, this also means that the edge states do not contribute to the linear *slope* of the FBCs and the slope comes solely from boundary contributions of extended bulk states which change as function of flux. We emphasize that while strong disorder can result in states that are fully localized in the system, numerically, we observe a substantial amount of bulk states that are extended over the whole system, including both boundaries. Finally, fully localized states in the spectrum are independent of the flux and do not contribute to the slope of the FBCs either.

Generally, the FBCs for the 2D system in the QHE regime exhibit all the four salient features which we have discussed in earlier sections. These features are also independent of the details of the profile functions $f_n^{L,R}$. All these findings highlight the robustness of the obtained results. The value of the linear slope c_ν is *universal* (independent of system parameters) and perfectly quantized in units of $e/2\pi$, $c_\nu = \nu e/2\pi$. All these suggest that this slope can be used as a topological invariant for the system. Importantly, in contrast to many other topological invariants such as winding numbers or Chern numbers which rely on the periodicity of the system and, thus, can be calculated only in the clean case, the topological invariant c_ν is well defined even in the presence of strong disorder in the whole system. In the next section we will establish the connections between c_ν and the quantized Hall conductance.

VI. FBC AND HALL CONDUCTANCE

In this section, we show that the FBC allows one to address explicitly the Hall conductance of the QHE system. For this we need to connect the FBC to the Hall current. We start by introducing the total charge of a small patch of area $\mathcal{A}$ located at the system boundary (see Fig. 6) as $Q_{\mathcal{A},2d} = Q_{\nu,2d}^L + Q_{\mathcal{A},2d}^b$, where $Q_{\mathcal{A},2d}^b$ is the bulk contribution defined as $Q_{\mathcal{A},2d}^b = \rho_\nu \mathcal{A}/a_x a_y$. We note that $Q_{\mathcal{A},2d}^b$ is independent of θ.

The continuity equation $\partial \rho_{2d}/\partial t + \boldsymbol{\nabla} \cdot \mathbf{j} = 0$ connects the charge density $\rho_{2d}(x, y) = e\langle \psi(x, y)^\dagger \psi(x, y)\rangle$ [continuum version of $\gamma_{n,m}$ given in Eq. (13)], with the current density $\mathbf{j}(x, y)$ in standard notation. Next, we integrate the equation over the patch $\mathcal{A}$ and use the Gauss theorem $\int_\mathcal{A} \boldsymbol{\nabla} \cdot \mathbf{j}\, d\mathcal{A} = \int_{\partial \mathcal{A}} \mathbf{j} \cdot d\mathbf{S}$, connecting the volume integral over the area $\mathcal{A}$ to the surface integral over the closed patch $\partial \mathcal{A}$. Here, the surface differential $d\mathbf{S}$ is a vector pointing normal to the boundary of the patch $\partial \mathcal{A}$. Thus, the continuity equation can be rewritten as

$$\frac{dQ_{\mathcal{A},2d}}{dt} + \int_{\partial \mathcal{A}} \mathbf{j} \cdot d\mathbf{S} = 0, \qquad (19)$$

where $Q_{\mathcal{A},2d} = \int_\mathcal{A} \rho_{2d}\, d\mathcal{A}$. For the patch located at the boundary of the system, only current along the x axis crossing the boundary between the patch and the bulk of the system I_x contributes to the integral. This allows us to define the total current $I_x = \int_{\partial \mathcal{A}} \mathbf{j} \cdot d\mathbf{S}$. From the continuity equation (19), we get $I_x = -\dot{Q}_{\mathcal{A},2d}$.

Next, we change the FBCs in time by changing the flux Φ through the cylinder. The bulk contribution $Q_{\mathcal{A},2d}^b$ stays constant and the change in the total charge is only due to the change in the FBC, $Q_{\nu,2d}^L$. Using Eq. (17), we obtain $\dot{Q}_{\mathcal{A},2d} = \dot{Q}_{\nu,2d}^L = c_\nu \dot{\theta} = 2\pi c_\nu \dot{\Phi}/\varphi_0$. According to the Faraday law, the change of flux in time generates the electromotive force $\mathcal{E}_y$ acting along the y axis, $\dot{\Phi} = -\mathcal{E}_y$. Combining the two expressions for the change of the FBC, we arrive at the following relation between the current I_x and the electromotive force $\mathcal{E}_y$:

$$I_x = -\frac{dQ_{\nu,2d}^L}{dt} = 2\pi c_\nu \frac{\mathcal{E}_y}{\varphi_0}. \qquad (20)$$

As a result, the Hall conductance σ_{xy} is given by

$$\sigma_{xy} = \frac{I_x}{\mathcal{E}_y} = \frac{2\pi c_\nu}{\varphi_0}. \qquad (21)$$
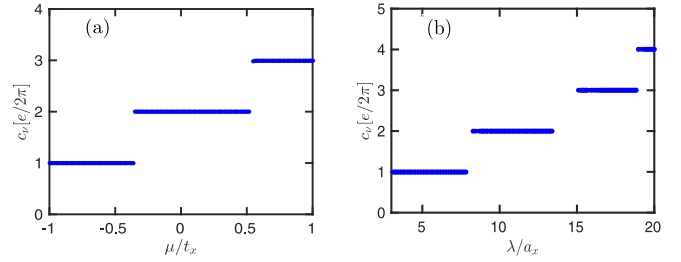

FIG. 9. The slope c_ν (in units of $e/2\pi$) (a) as function of the position of the chemical potential μ and (b) as a function of $\lambda = h/eBa_y$. We focus on the isotropic regime with $t_y/t_x = 1$ and fix either (a) the magnetic field $\lambda/a_x = 10$ or (b) the position of the chemical potential $\mu/t_x = 0$. The remaining parameter values are chosen as in Fig. 7. The quantization of the slope c_ν results in quantized plateaus in the Hall conductance σ_{xy}.

Using the values of the linear slope $c_\nu = \frac{e\,\nu}{2\pi}$ found above both analytically and numerically, we find that the conductance takes the form $\sigma_{xy} = \frac{\nu e^2}{h}$, which are the quantized values of the integer QHE.

Remarkably, the linear slope of the FBCs takes quantized value that leads to the quantized Hall conductance. We also compute numerically the dependence of c_ν (and thus of the Hall conductance σ_{xy}) on the position of the chemical potential as well as on λ (which is inversely proportional to magnetic field B) (see Fig. 9). The slope c_ν is an integer multiple of $e/2\pi$ inside a given gap. As one increases μ or λ, more bands get filled and c_ν changes by $e/2\pi$ as one of the bulk bands crosses the chemical potential (see Fig. 2). The plateaus in c_ν correspond to plateaus in the Hall conductance σ_{xy} and they are stable against disorder as shown in the previous section. Therefore, our approach gives an alternative way to microscopically understand the Hall conductance and its robust quantization. As seen in previous sections, the slope of the FBCs has contributions from all occupied bands. Thus, also the Hall conductance gets contributions from all occupied bands, except from the edge states. Also, the linear slopes of the FBCs imply that the Hall current is stationary. In our approach, we continuously (and adiabatically) vary the flux between two arbitrary values and can clearly see that the Hall current is stationary. However, in Laughlin's argument one considers the variation of the flux only by an integer value of φ_0 and thereby must also assume that the current is stationary for all flux values *between* $n\varphi_0$ and $(n + 1)\varphi_0$, for integer n. Thus, our approach shows that the linear slopes reflect the fact that the Hall current is stationary.

We note that our approach is also valid for finite temperatures as long as the temperature stays smaller than the energy distance from the chemical potential to the nearest bulk band (see Appendix E). As soon as the temperature is high enough to thermally excite electrons from localized edge states to extended bulk states (or vice versa), the FBCs cannot be defined properly anymore. As a result, the linear dependence of the FBCs on the flux breaks down. Hence, as the temperature increases, the Hall plateaus begin to shrink before disappearing eventually.

We also would like to emphasize the advantages of the approach presented here over the Laughlin argument [4]. First,

the change in the flux Φ does not need to be an integer multiple of the flux quantum φ_0 as assumed in Laughlin's argument [4], but instead can take any value. Second, and more important, our derivation is valid also in systems with strong disorder, whereby the disorder can be present in the whole sample including the boundaries. The linear dependence of the FBCs on the magnetic flux holds also in this case, which highlights the remarkable stability of the quantized values against disorder. This stability suggests that the slope c_ν of the FBCs plays the role of a topological invariant which is well defined even in the presence of strong disorder. Finally, we note that our derivation is valid for any position of the chemical potential inside the bulk gap (see Fig. 9).

VII. CONCLUSIONS AND OUTLOOK

We have studied FBCs occurring in one-dimensional nanowires with periodically modulated chemical potential as well as in two-dimensional electron gases in the presence of a perpendicular magnetic field in the integer QHE regime. In the clean limit, these two systems can be mapped onto each other. In both systems, the FBCs are linear functions of the phase offset (1D case) or of the magnetic flux in the cylinder topology of the Laughlin setup (2D case). This linear slope c_ν depends only on the number of filled bulk bands but not on the precise position of the chemical potential inside these bands. The slope is universal and quantized in units of $e/2\pi$ and, moreover, is also extremely robust against disorder. Interestingly, c_ν is determined solely by bulk bands, while the bound states in 1D or the chiral edge states in 2D are responsible for the jumps in the FBCs, which are quantized in units of e. We have shown that all these features are robust against disorder, and thus one can consider c_ν as a topological invariant that is well defined even in the presence of strong disorder.

In addition, we have shown that the direct consequence of quantized values of the slope c_ν is the quantization of the Hall conductance. Our derivation is performed for the Laughlin cylinder setup and, thus, can be tested experimentally in the Corbino disk geometry. As only the bulk states are responsible for the finite slope c_ν, we conclude that the Hall current is carried by extended bulk states. The FBCs and their change as function of phase offset in NWs or of flux in Corbino disks can be tested experimentally by making use of, for example, single-electron transistors [70,71] as charge sensors. As an outlook, it would be interesting to generalize our approach to the Hall bar geometry.

APPENDIX A: EFFECTIVE HAMILTONIAN FOR NW IN HIGHER-ORDER PERTURBATION THEORY IN V

In this appendix, we calculate explicitly the effective Hamiltonian describing the coupling between right and left

movers at the Fermi surface in the case of higher-order resonances $k_F = \nu\pi/\lambda$ in the perturbative regime with $V \ll t_x$, as specified in the main part. Generally, the only nonzero matrix elements of $H_{\rm CDW}$ [Eq. (4)] in momentum space M_{k_1,k_2} are the ones that connect two states with the momentum difference $2\pi/\lambda$:

$$M_{k_1,k_2} = \langle k_1|H_{\rm CDW}|k_2\rangle$$
$$= -V\,e^{i\alpha}\delta_{k_1,k_2-2\pi/\lambda} - V\,e^{-i\alpha}\delta_{k_1,k_2+2\pi/\lambda}. \quad (A1)$$

As a result, if $k_F = \nu\pi/\lambda$, the gap at the Fermi surface $\Delta_g^{(\nu)}$ can be opened in the νth-order perturbation theory [63,64]. In this case, the effective Hamiltonian density in momentum space and in the basis $\tilde\psi = (R, L)$ is defined as

$$\mathcal{H}^{(\nu)} = \begin{pmatrix} \hbar\,v_F^{(\nu)}\,k & \bar\Delta_g^{(\nu)} \\ (\bar\Delta_g^{(\nu)})^* & -\hbar\,v_F^{(\nu)}\,k \end{pmatrix}, \quad (A2)$$

with the Fermi velocity given by $v_F^{(\nu)} = 2\,t_x\,a_x\,\sin(k_F a_x)/\hbar$. The matrix element $\bar\Delta_g^{(\nu)}$ connecting the right mover at the momentum k_F and the left mover at the momentum $-k_F$ is found in the νth-order perturbation expansion in V as

$$\bar\Delta_g^{(\nu)} \equiv \Delta_g^{(\nu)}e^{i\nu\alpha}$$
$$= \frac{M_{k_F,k_F-2\pi/\lambda}\cdots M_{-k_F-4\pi/\lambda,-k_F-2\pi/\lambda}M_{-k_F-2\pi/\lambda,-k_F}}{\prod_{q=1}^{\nu-1}\left[E_{-k_F}^0 - E_{-k_F+2\pi q/\lambda}^0\right]}$$
$$= \frac{V^\nu e^{i\nu(\alpha+\pi)}}{(4\,t_x)^{\nu-1}\prod_{q=1}^{\nu-1}\sin^2(k_F a_x q/\nu)}, \quad (A3)$$

where $E_k^0 = 2\,t_x[1 - \cos(k\,a_x)]$ is the energy dispersion of the unperturbed Hamiltonian consisting only of the kinetic part. The spectrum of the effective Hamiltonian is given by $E_\pm = \pm[(\hbar\,v_F^{(\nu)}\,k)^2 + (\Delta_g^{(\nu)})^2]$. The gap of the size $\Delta_g^{(\nu)} \sim V^\nu/E_0^{\nu-1}$ is opened at the Fermi surface. Here, to simplify estimates, we introduced the characteristic energy E_0, which depends on the position of the chemical potential and is of order of the Fermi energy.

We note that Eq. (A2) obtained in the νth order of the perturbation theory maps back to the one considered in the main text ($\nu = 1$) if one rescales $\alpha \to \nu\alpha$ and $V \to \Delta_g^{(\nu)}$. As a direct consequence, the number of bound states observed at any given energy inside the bulk gap as one tunes α from $-\pi$ to π is also increased from one to ν (see Fig. 2).

APPENDIX B: INDEPENDENCE OF FBCs ON CHOICE OF CUTOFFS n_1 AND n_2

In this appendix, we demonstrate numerically that the FBCs are a well-defined quantity that do not depend on the choice of cutoffs n_1 and n_2 as long as $n_1 a_x > \xi$ and $n_2 a_x > \lambda$ (see Fig 10). The first condition $n_1 a_x > \xi$ ensures that the summation is done over the whole extension of the bound state (characterized by its localization length ξ) such that the difference in the FBC for this state being occupied or not is given by e. The second condition $n_2 a_x > \lambda$ ensures that the FBC is averaged over several unit cells as the charge distribution inside the unit cell even in the bulk (away from the end of the NW) is nonuniform if the chemical potential is periodically modulated [41].
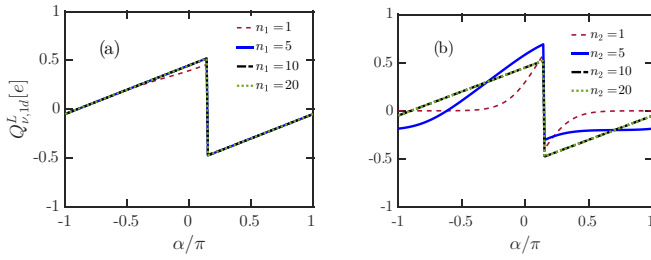
FIG. 10. The FBCs, $Q_{\nu,1d}^{L}$, as a function of the phase offset α obtained numerically for the CDW-modulated NW for different cutoffs: (a) $n_1 = 1$ (red), 5 (blue), 10 (black), 20 (green), and $n_2 = 10$; (b) $n_1 = 10$ and $n_2 = 1$ (red), 5 (blue), 10 (black), 20 (green). The slope of the FBC is independent of the cutoffs as long as $n_1 a_x > \xi$ and $n_2 a_x > \lambda$. The number of filled bands is controlled by the chemical potential, which is tuned inside the first bulk gap $\nu = 1$ (see Fig. 2). Other parameters are chosen to be the same as in Fig. 2 of the main text.

APPENDIX C: PARTICLE DENSITIES FOR $\nu = 2, 3$

In addition, we explore the profile of the local particle density γ_n^{θ} for different numbers of filled bands (see Fig. 11). In the bulk, γ_n^{θ} does not depend on θ. In contrast to that, at the boundaries, γ_n^{θ} is sensitive to the flux, giving rise to the linear slope in the θ dependence of the FBCs.

APPENDIX D: FBCs IN 2D MODELS WITH DIFFERENT DEGREE OF ANISOTROPY t_y/t_x

In this appendix we address the stability of the results against variations in the relative strengths of the hopping amplitudes in the 2D model. In particular, we numerically calculate the FBCs for different ratios t_y/t_x (see Fig. 12). This allows us to tune from the isotropic regime with $t_y = t_x$ to the highly anisotropic model with $t_y \ll t_x$ [50,68,69,72–82]. The obtained slopes in the FBCs are always quantized and independent of the ratio t_y/t_x, and, moreover, they are stable against disorder as long as the band gap is well defined. Our results clearly show that the features of the FBCs as well as the resulting quantized values of the Hall conductance are independent of the anisotropy of the model.
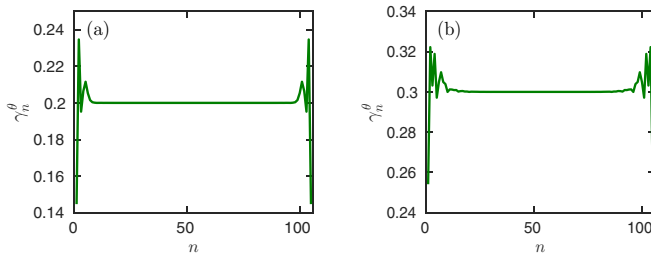

FIG. 11. Local particle density γ_n^{θ} as a function of position along the NW. The chemical potential lies (a) in the second ($\nu = 2$) bulk gap with $\mu/t_x = 0.5$ or (b) in the third ($\nu = 3$) bulk gap with $\mu/t_x = 1$. The particle densities are constant in the bulk but nonuniform at the boundaries. Other parameter values are the same as in Fig. 7(a) of the main text.
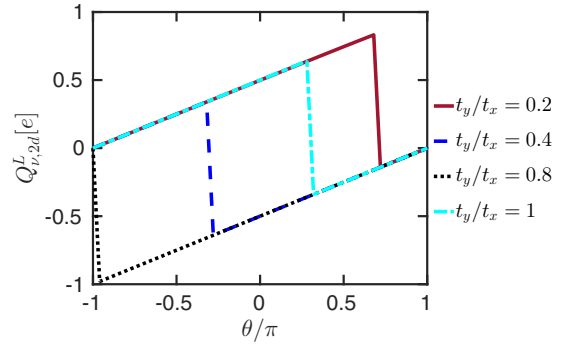

FIG. 12. The FBCs, $Q_{\nu,2d}^{L}$, as a function of the flux phase θ for different values of the hopping amplitude between NWs: $t_y/t_x = 1$ (cyan), 0.8 (black), 0.4 (blue), and 0.2 (red). The chemical potential μ is tuned into the first bulk gap ($\nu = 1$): $\mu/t_x = -0.7, -0.5, 0$, and 0.2, respectively. We observe the linear dependence of $Q_{\nu,2d}^{L}$ on θ. The slope c_ν is quantized and independent of whether the system is isotropic or not. The remaining parameter values are the same as in Fig. 7 of the main text.

APPENDIX E: FBCs AT FINITE TEMPERATURES

In this appendix, we study numerically the FBCs at finite temperature T (see Fig. 13). For this we modify the definition of the FBCs introduced in Eq. (14), where only states with negative energies contributed to the FBCs. At finite temperatures, the weight of each state with energy ϵ_p is given by the Fermi-Dirac distribution function $\tilde{n}(\epsilon_p) = 1/[1 + \exp(\epsilon_p/k_B T)]$, where the index p labels the $M \times N$ states of the tight-binding Hamiltonian H^{θ} given in Eq. (15), and k_B is the Boltzmann constant. The corresponding wave functions are given by $\tilde{\phi}_p(n, m)$. The important parameters describing the effect of temperature are the energy distance Δ between the chemical potential and the nearest bulk band. If $k_B T/\Delta \ll 1$, the slope c_ν is perfectly linear. As temperature
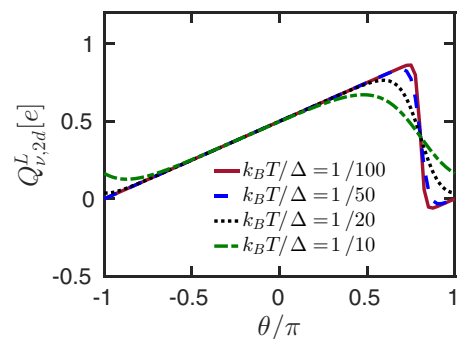

FIG. 13. The FBCs, $Q_{\nu,2d}^{L}$, as a function of the flux phase θ at different temperatures: $k_B T/\Delta = 1/100$ (red), 1/50 (blue), 1/20 (black), and 1/10 (green). All parameters are the same as in Fig. 7(d). Here, Δ is the energy distance between the chemical potential and the nearest bulk band. For the chemical potential tuned inside the first ($\nu = 1$) bulk gap (yellow solid line in Fig. 2), the energy distance to the second band is $\Delta/t = 0.16$. We still observe the linear dependence of $Q_{\nu,2d}^{L}$ on θ, however, the jump in the FBC gets smoother as the temperature increases, which makes it more difficult to define the slope c_ν. If $k_B T$ gets close to Δ, the linear dependence of the FBC on the flux disappears.

is increased, the jump in $Q^s_{\nu,2d}$ gets smoother and the dependence of FBCs on the flux phase θ is linear only sufficiently far away from the jump (see Fig. 13). As $k_B T$ is increased further and gets close to Δ, the electron gets thermally excited from (into) a localized edge state into (from) extended bulk states separated by the gap Δ. As a result, the definition of

the FBCs assumed to be a property of the boundaries breaks down. This has an effect on c_ν as well as the quantized Hall conductance (see Fig. 9). The thermal broadening of the plateaus does not allow one to observe the quantization any longer if $k_B T \approx \Delta$. Thus, the plateaus will first shrink and eventually disappear as one increases the temperature.

---

[1] K. V. Klitzing, G. Dorda, and M. Pepper, Phys. Rev. Lett. **45**, 494 (1980).

[2] D. C. Tsui, H. L. Stormer, and A. C. Gossard, Phys. Rev. Lett. **48**, 1559 (1982).

[3] D. J. Thouless, M. Kohmoto, M. P. Nightingale, and M. den Nijs, Phys. Rev. Lett. **49**, 405 (1982).

[4] R. B. Laughlin, Phys. Rev. Lett. **50**, 1395 (1983).

[5] J. K. Jain, Phys. Rev. Lett. **63**, 199 (1989).

[6] R. E. Prange and S. M. Girvin, *The Quantum Hall Effect* (Springer, New York, 1990).

[7] A. H. McDonald, *Quantum Hall Effect: A Perspective* (Kluwer Academic, Dordrecht, 1990).

[8] J. K. Jain, *Composite Fermions* (Cambridge University Press, Cambridge, 2007).

[9] F. D. M. Haldane, Phys. Rev. Lett. **51**, 605 (1983).

[10] B. I. Halperin, Phys. Rev. Lett. **52**, 1583 (1984).

[11] R. Willett, J. P. Eisenstein, H. L. Störmer, D. C. Tsui, A. C. Gossard, and J. H. English, Phys. Rev. Lett. **59**, 1776 (1987).

[12] G. Moore and N. Read, Nucl. Phys. B **360**, 362 (1991).

[13] R. Jackiw and C. Rebbi, Phys. Rev. D **13**, 3398 (1976).

[14] R. Jackiw and J. Schrieffer, Nucl. Phys. B **190**, 253 (1981).

[15] W. P. Su, J. R. Schrieffer, and A. J. Heeger, Phys. Rev. Lett. **42**, 1698 (1979).

[16] W. P. Su and J. R. Schrieffer, Phys. Rev. Lett. **46**, 738 (1981).

[17] J. Goldstone and F. Wilczek, Phys. Rev. Lett. **47**, 986 (1981).

[18] M. J. Rice and E. J. Mele, Phys. Rev. Lett. **49**, 1455 (1982).

[19] R. Jackiw and G. Semenoff, Phys. Rev. Lett. **50**, 439 (1983).

[20] S. Kivelson, Phys. Rev. B **28**, 2653 (1983).

[21] R. de-Picciotto, M. Reznikov, M. Heiblum, V. Umansky, G. Bunin, and D. Mahalu, Nature (London) **389**, 162 (1997).

[22] L. Saminadayar, D. C. Glattli, Y. Jin, and B. Etienne, Phys. Rev. Lett. **79**, 2526 (1997).

[23] H. Steinberg, G. Barak, A. Yacoby, L. N. Pfeiffer, K. W. West, B. I. Halperin, and K. Le Hur, Nat. Phys. **4**, 116 (2007).

[24] H. Inoue, A. Grivnin, N. Ofek, I. Neder, M. Heiblum, V. Umansky, and D. Mahalu, Phys. Rev. Lett. **112**, 166801 (2014).

[25] X.-L. Qi, T. L. Hughes, and S.-C. Zhang, Nat. Phys. **4**, 273 (2008).

[26] S. Ryu, C. Mudry, C.-Y. Hou, and C. Chamon, Phys. Rev. B **80**, 205319 (2009).

[27] N. Goldman, I. Satija, P. Nikolic, A. Bermudez, M. A. Martin-Delgado, M. Lewenstein, and I. B. Spielman, Phys. Rev. Lett. **105**, 255302 (2010).

[28] J. C. Budich and E. Ardonne, Phys. Rev. B **88**, 035139 (2013).

[29] Z. Xu, L. Li, and S. Chen, Phys. Rev. Lett. **110**, 215301 (2013).

[30] F. Grusdt, M. Höning, and M. Fleischhauer, Phys. Rev. Lett. **110**, 260405 (2013).

[31] J. Klinovaja and D. Loss, Phys. Rev. Lett. **110**, 126402 (2013).

[32] K. A. Madsen, E. J. Bergholtz, and P. W. Brouwer, Phys. Rev. B **88**, 125118 (2013).

[33] A. V. Poshakinskiy, A. N. Poddubny, L. Pilozzi, and E. L. Ivchenko, Phys. Rev. Lett. **112**, 107403 (2014).

[34] D. Rainis, A. Saha, J. Klinovaja, L. Trifunovic, and D. Loss, Phys. Rev. Lett. **112**, 196803 (2014).

[35] J. Klinovaja and D. Loss, Phys. Rev. Lett. **112**, 246403 (2014).

[36] R. Wakatsuki, M. Ezawa, Y. Tanaka, and N. Nagaosa, Phys. Rev. B **90**, 014505 (2014).

[37] G. van Miert and C. Ortix, Phys. Rev. B **96**, 235130 (2017).

[38] B. Pérez-González, M. Bello, A. Gómez-León, and G. Platero, arXiv:1802.03973.

[39] M. Serina, D. Loss, and J. Klinovaja, Phys. Rev. B **98**, 035419 (2018).

[40] S. Gangadharaiah, L. Trifunovic, and D. Loss, Phys. Rev. Lett. **108**, 136803 (2012).

[41] J.-H. Park, G. Yang, J. Klinovaja, and P. Stano, and D. Loss, Phys. Rev. B **94**, 075416 (2016).

[42] D. J. Thouless, Phys. Rev. B **27**, 6083 (1983).

[43] Q. Niu, Phys. Rev. Lett. **64**, 1812 (1990).

[44] D. Xiao, M.-C. Chang, and Q. Niu, Rev. Mod. Phys. **82**, 1959 (2010).

[45] Y. E. Kraus, Y. Lahini, Z. Ringel, M. Verbin, and O. Zilberberg, Phys. Rev. Lett. **109**, 106402 (2012).

[46] L. Wang, M. Troyer, and X. Dai, Phys. Rev. Lett. **111**, 026802 (2013).

[47] P. Marra, R. Citro, and C. Ortix, Phys. Rev. B **91**, 125411 (2015).

[48] T. Ozawa, H. M. Price, N. Goldman, O. Zilberberg, and I. Carusotto, Phys. Rev. A **93**, 043827 (2016).

[49] O. Zilberberg, S. Huang, J. Guglielmon, M. Wang, K. P. Chen, Y. E. Kraus, and M. C. Rechtsman, Nature (London) **553**, 59 (2018).

[50] J. Klinovaja and D. Loss, Phys. Rev. Lett. **111**, 196401 (2013).

[51] B. I. Halperin, Phys. Rev. B **25**, 2185 (1982).

[52] D. A. Syphers, K. P. Martin, and R. J. Higgins, Appl. Phys. Lett. **48**, 293 (1986).

[53] P. F. Fontein, J. M. Lagemaat, J. Wolter, and J. P. André, Semicond. Sci. Technol. **3**, 915 (1988).

[54] V. T. Dolgopolov, A. A. Shashkin, N. B. Zhitenev, S. I. Dorozhkin, and K. von Klitzing, Phys. Rev. B **46**, 12560 (1992).

[55] M. J. Zhu, A. V. Kretinin, M. D. Thompson, D. A. Bandurin, S. Hu, G. L. Yu, J. Birkbeck, A. Mishchenko, I. J. Vera-Marun, K. Watanabe, T. Taniguchi, M. Polini, J. R. Prance, K. S. Novoselov, A. K. Geim, M. Ben Shalom, Nat. Commun. **8**, 14552 (2017).

[56] B. A. Schmidt, K. Bennaceur, S. Gaucher, G. Gervais, L. N. Pfeiffer, and K. W. West, Phys. Rev. B **95**, 201306(R) (2017).

[57] R. A. Deutschmann, W. Wegscheider, M. Rother, M. Bichler, G. Abstreiter, C. Albrecht, and J. H. Smet, Phys. Rev. Lett. **86**, 1857 (2001).

[58] R. E. Algra, M. A. Verheijen, M. T. Börgstrom, L.-F. Feiner, G. Immink, W. J. van Enckevort, E. Vlieg, and E. P. Bakkers, Nature (London) **456**, 369 (2008).

[59] B. Braunecker, G. I. Japaridze, J. Klinovaja, and D. Loss, Phys. Rev. B **82**, 045127 (2010).

[60] J. Klinovaja and D. Loss, Phys. Rev. B **86**, 085408 (2012).

[61] J. Klinovaja, P. Stano, and D. Loss, Phys. Rev. Lett. **109**, 236801 (2012).

[62] D. Rainis, L. Trifunovic, J. Klinovaja, and D. Loss, Phys. Rev. B **87**, 024515 (2013).

[63] M. Thakurathi, W. DeGottardi, D. Sen, and S. Vishveshwara, Phys. Rev. B **85**, 165425 (2012).

[64] M. Thakurathi, D. Sen, and A. Dutta, Phys. Rev. B **86**, 245424 (2012).

[65] I. Tamm, Z. Phys. **76**, 849 (1932).

[66] W. Shockley, Phys. Rev. **56**, 317 (1939).

[67] V. M. Yakovenko, Phys. Rev. B **43**, 11353 (1991).

[68] C. L. Kane, R. Mukhopadhyay, and T. C. Lubensky, Phys. Rev. Lett. **88**, 036401 (20012).

[69] J. Klinovaja and D. Loss, Eur. Phys. J. B **87**, 171 (2014).

[70] S. Ilani, J. Martin, E. Teitelbaum, J. H. Smet, D. Mahalu, and V. Umansky, and A. Yacoby, Nature (London) **427**, 328 (2004).

[71] J. Martin, N. Akerman, G. Ulbricht, T. Lohmann, J. H. Smet, and K. von Klitzing, and A. Yacoby, Nat. Phys. **4**, 144 (2008).

[72] D. Poilblanc, G. Montambaux, M. Héritier, and P. Lederer, Phys. Rev. Lett. **58**, 270 (1987).

[73] L. P. Gorkov and A. G. Lebed, Phys. Rev. B **51**, 3285 (1995).

[74] M. Horsdal and J. M. Leinaas, Phys. Rev. B **76**, 195321 (2007).

[75] J. C. Y. Teo and C. L. Kane, Phys. Rev. B **89**, 085101 (2014).

[76] I. Seroussi, E. Berg, and Y. Oreg, Phys. Rev. B **89**, 104523 (2014).

[77] J. Klinovaja and Y. Tserkovnyak, Phys. Rev. B **90**, 115426 (2014).

[78] T. Meng and E. Sela, Phys. Rev. B **90**, 235425 (2014).

[79] E. Sagi and Y. Oreg, Phys. Rev. B **90**, 201102 (2014).

[80] J. Klinovaja, Y. Tserkovnyak, and D. Loss, Phys. Rev. B **91**, 085426 (2015).

[81] T. Meng, T. Neupert, M. Greiter, and R. Thomale, Phys. Rev. B **91**, 241106 (2015).

[82] P. Szumniak, J. Klinovaja, and D. Loss, Phys. Rev. B **93**, 245308 (2016).